Signal Propagation Characteristics between Transceivers on Human Body for MHz-Band Near-Field Coupling Communication

Masaki Ishida[1], Tomonori Nakamura[1], Mami Nozawa[1], Naoto Watanabe[1], Hitoshi Shimasaki[1], Yuichi Kado[1], and Mitsuru Shinagawa[2]

1 Department of Electronics, Kyoto Institute of Technology, Hashigami-cho Matsugasaki Sakyo-ku, Kyoto, Japan

E-mail: kado@kit.ac.jp

2 Faculty of Science and Engineering, Hosei University, 3-7-2, Kajino-cho, Koganei-shi, Tokyo, Japan

E-mail: m.shina@hosei.ac.jp

ABSTRACT

A method is presented for precisely evaluating signal propagation loss on the human body between transceivers in near–field coupling communication (NFCC) that uses the surface of the human body as a transmission path. It is important to assess the loss of signal propagation on the human body to design stable and reliable NFCC networks. We measured signal intensity to compare two methods of measurement with a battery-powered transmitter and an AC-powered signal generator. The results revealed that the AC-powered signal generator affected the communication path. Furthermore, we successfully found a distance dependence of signal loss between transceivers on the human body. We clarified the necessity for properly setting the transmitter power and receiver sensitivity that corresponded to the distance dependence of signal loss.

Categories and Subject Descriptors

B.4.1 [**INPUT/OUTPUT AND DATA COMMUNICATIONS**]: Data Communications Devices – *Receivers, Transmitters.*
B.4.2 [**INPUT/OUTPUT AND DATA COMMUNICATIONS**]: Input / Output Devices -*Channels and controllers*

General Terms

Measurement, Design, Reliability, Experimentation, Security, Human Factors, Standardization

Keywords

Near-field coupling communication, Electrically isolated measurement, Path/Signal loss, Electrical-to-optical and optical-to-electrical conversion.

1. INTRODUCTION

Wireless body area networks (WBANs) around the human body represent a promising technology for new applications in areas like secure systems, intelligent transportation systems, medical information systems, and payment systems as concerns over safety, security, and health have been increasing in our aging society. Body-channel communication (BCC) technology, which is one of the physical layers used to standardize wireless body-area networks (WBANs), has recently been actively researched [1]–[4]. We have been investigating near–field coupling communication (NFCC) technology that uses the surface of the human body as a data transmission path with modulated electrostatic field signals induced on the surface of the human body. This technology is composed of two types of transceivers on the human body (wearable TRXs) and those embedded in environments or in equipment (embedded TRXs) [5]. Security and usability in the health management of patients are required in hospital scenarios. The main advantage of NFCC using the MHz-band is its short radial distance, which enables us to establish an intuitive "touch and connect" form of communication. The frequency is below 10 MHz to utilize this advantage. From this point of view, NFCC is efficient in the medical field where the leaking of personal information of patients and radio jamming must be avoided.

Fig. 1 shows its applications in a hospital. Patients are wearing wearable TRXs and the electrodes connected to an embedded TRX are embedded under the floor or inside a door. The wearable TRXs and the embedded TRX mutually communicate information by using the surface of the human body as a data transmission path only when the patient touches or steps on the embedded electrodes. Since the electrodes are embedded in various places in hospitals, doctors and nurses can monitor the patient's position and health condition from a nurse station.

It is important to assess signal loss in the path from the transmitter (TX) to the receiver (RX) and model the communication path to achieve stable communication. We have already reported signal transmission between wearable and embedded TRXs [6]. However, communications between multiple nodes on the body are required to collect some vital information for the application in Fig. 1. Therefore, we tried measuring signal loss between wearable TRXs on the human body.

BODYNETS 2013, September 30-October 02, Boston, United States

DOI 10.4108/icst.bodynets.2013.253682

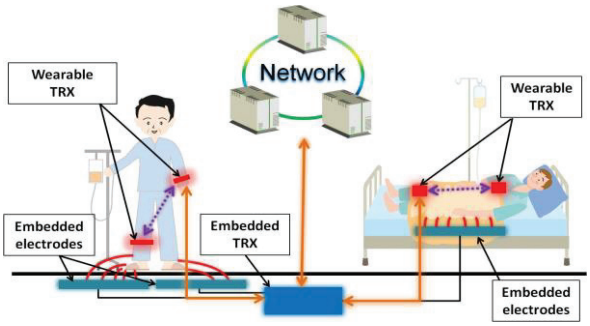

Figure 1. Medical applications in hospital.

2. SIGNAL PATH MODELS

2.1 Equivalent Circuits

Two types of signal path models for the NFCC system between wearable TRXs are outlined in Figs. 2 (a) and (b), which describe the patterns of a reclining and standing human body. Where C_{a1} and C_{b1} are between ground electrodes of TRXs, C_{a2}, C_{b2}, C_{a3}, and C_{b3} are between the ground electrode of a TRX and floor ground, C_{a4}, C_{b4}, C_{a5}, and C_{b5} are between the signal electrode of a TRX and the human body, C_{a6}, C_{b6}, C_{a7}, and C_{b7} are between the ground electrode of a TRX and the human body, and C_{a8} and C_{b8} are between the human body and floor ground [7]. The first wearable TRX induces a modulated quasi-electrostatic field signal on the human body through a mechanism for near-field coupling, and communication occurs when the second wearable TRX detects the signal from the first. These TRXs allow two-way communication. The signal loop consists of two types of paths, which are a forward and a return path as shown in Fig.2. We regard the human body as a conductor in the 6.75 MHz frequency range used for communication. However, there are variable coupling capacitances that emanate from shoes and clothes. Path loss depends on these capacitances. Therefore, as it is difficult to define path loss clearly with numerical methods, we need to estimate this experimentally to design stable communication links.

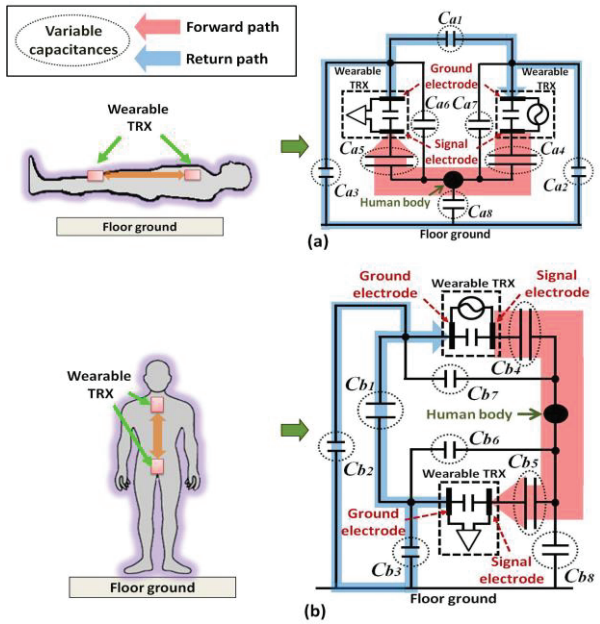

Figure 2. (a) and (b) Equivalent circuits and signal path models.

2.2 Problem with Conventional Measurement System

This section describes the main problem with conventional measurement systems using an AC-powered signal generator for estimating the signal propagation loss on the surface of the human body as shown in Fig. 3 (a). The signal generator induces an electrical signal on a pair of parallel electrodes through the coaxial cable. The electrodes have the same size and shape as those of the wearable TRX. The signal line and ground line of the coaxial cable are connected to the signal and ground electrodes. The ground line is also connected to the signal ground input of the signal generator. The external ground of the AC-powered signal generator is connected to the floor ground. Fig. 3 (b) has an equivalent circuit for the measurement system using a generator instead of the wearable TRX when the distance between the wearable TRXs is more than 30 mm. The return path through C_{a2} and C_{a3} dominates rather than that through C_{a1} under these conditions. When an AC-powered signal generator is connected to the pair of electrodes through a coaxial cable, low impedance Z occurs between the ground electrode and floor ground. Impedance Z is composed of parasitic capacitances due to the housing of the generator and the coaxial cable. Note that the return path of the signal loop is enhanced by the additional low impedance compared with the return path in Fig. 2 (a). Therefore, we need to design and build a battery-powered TX of the same size as that of the wearable TRX we developed.

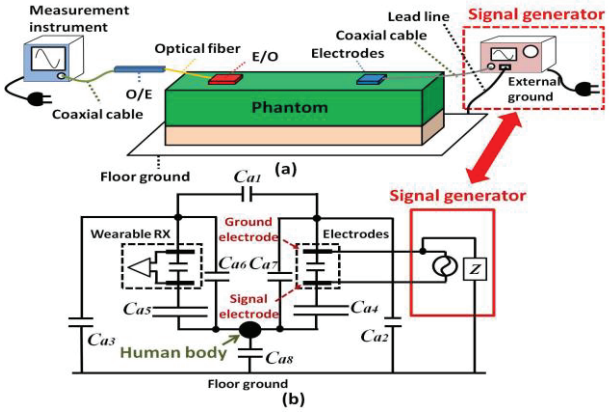

Figure 3. (a) Schematic of setup and (b) equivalent circuit for conventional measuring system.

3. MEASUREMENT INSTURUMENTS

3.1 Battery-Powered TX

We developed a battery-powered TX that generates a sinusoidal wave signal of about 10 $V_{p\text{-}p}$ at 6.75 MHz. Figs. 4 (a) and (b) are a photograph and a block diagram of the TX. The sinusoidal wave signal was created by the crystal oscillator, transmitted through the amplifier for impedance transformation, and was fed into the electrodes. The dimensions of the TX were 85 x 54 x 6.5 mm. The signal electrode in the TX was 36.8 cm^2 and the ground electrode was 19.5 cm^2. They were exactly the same as those in the wearable TRX that we developed shown in Fig. 4 (c).

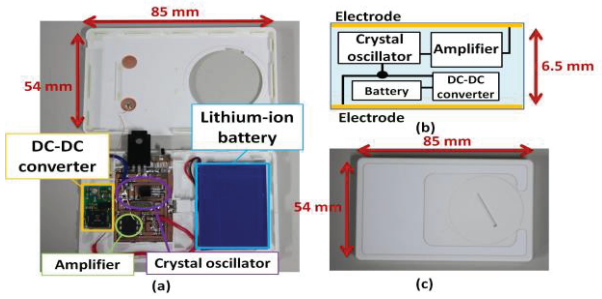

Figure 4. (a) Photograph of battery-powered TX, (b) block diagram of battery-powered TX, and (c) photograph of the developed wearable TRX.

3.2 E/O and O/E Probe

We designed and built a probe to accurately measure the received signal of a wearable TRX consisting of an electrical-to-optical (EO) converter and an optical-to-electrical (OE) converter. Fig. 5 has a block diagram of the EO-OE probe. The probe head receives the signal. The electrodes are parallel plates and are of the same size as those in the wearable TRX. E/O circuit converts the electrical signal to an optical signal and O/E circuit reconverts the optical signal to an electrical signal. The signals between the two devices propagate in the optical fiber. In addition, the circuit E/O is driven by a battery, and the circuit O/E is driven by a DC source. The circuit gain of the EO-OE probe is 23.8 dB at 6.75 MHz.

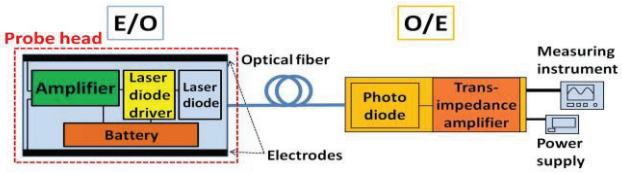

Figure 5. Block diagram of E/O and O/E probe

4. EXPERIMENTS AND RESULTS

We measured signal loss caused between the TX and RX on a phantom, which imitated the two patterns of the human body of reclining and standing. We chose a spectrum analyzer as the measurement instrument, which was battery-powered. We used a phantom that had the same electrical properties as those of the human body. The content of the phantom is a gel material with a conductivity of 0.59 S/m at 6.75 MHz (human body: 0.60 S/m) [8] and packed by a plastic sheet. The phantom's dimensions were 95 x 19 x 19 cm. We transmitted a sinusoidal wave of 6.75 MHz to the electrodes by using an AC-powered signal generator (AC-powered TX) and battery-powered TX in the experiments. The external ground of the signal generator was connected to the floor ground by a lead line. These TXs were fixed in position and the EO-OE probe head was moved on the phantom. We measured the received voltage of the EO-OE probe and calculated the path loss, which was represented by the ratio of the received voltage to the transmission voltage defined as:

$$\text{Loss} = 20 \times \log\left\{\frac{\textit{Received voltage}}{\textit{Transmission voltage}}\right\}[\text{dB}] \qquad (1)$$

The first pattern assumed a situation where a human body wearing two TRXs was lying on a bed. Figs. 6 (a) and (b) are a schematic of the experimental systems. A polystyrene board with a thickness of 100 mm was positioned between the phantom and the floor ground. It had the same electrical characteristics as air and was assumed to be bedding on a bed. The distance between the TX and the EO-OE probe head was d_1.

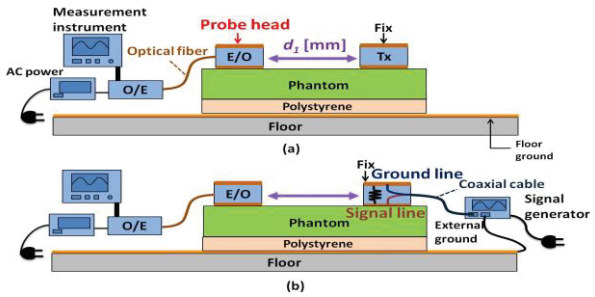

Figure 6. (a) and (b) Setup for experiments on reclining phantom.

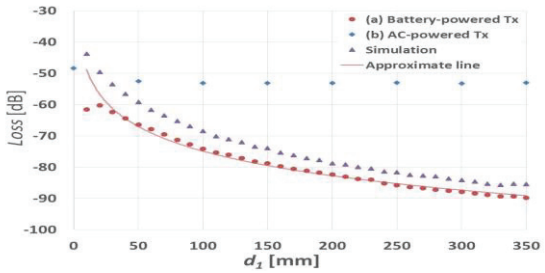

Figure 7. Path loss according to distance on surface of reclining phantom.

Fig. 7 plots the path loss caused between the AC-powered or battery-powered TXs and the EO-OE probe head for the reclining phantom. As the distance between the EO-OE probe head and the battery-powered TX increased, the received signals became smaller. In contrast, the measured values using the AC-powered TX were almost constant. These results revealed that the AC-powered TX had a problem with overestimating the signals and that there was a distance dependence of signal loss between the TRXs on the human body. When the distance between the TX and the probe head was longer than 30 mm, return path through C_{a1} was dominant rather than the return path through C_{a2} and C_{a3}. So, the received signal intensity mainly varied in accordance with the magnitude of C_{a1}, which caused a distance dependence of path loss.

On the other hand, the next pattern assumed a situation where a human body wearing two TRXs was standing on the floor. Figs. 8 (a) and (b) are a schematic of the experimental systems, where the phantom, the EO-OE probe, and the AC-powered and battery-powered TXs are the same as those we used previously. The distance between the TX and the EO-OE probe head was d_2.

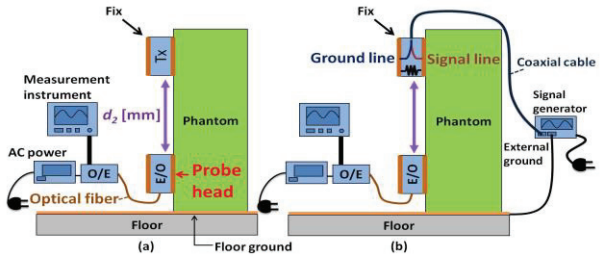

Figure 8. (a) and (b) Setup for experiments on standing phantom.

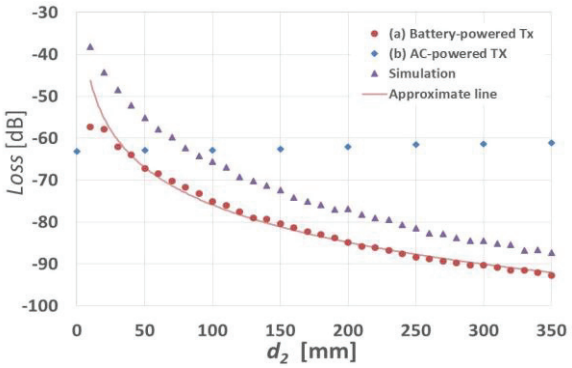

Figure 9. Path loss according to distance on surface of standing phantom.

Fig. 9 plots the path loss between the AC-powered or battery-powered TXs and the EO-OE probe head for the standing phantom. The closer the EO-OE probe head was to the battery-powered TX, the larger the path loss was. In contrast, the measured values using the EO-OE probe and the AC-powered TX were constant. The closer the EO-OE probe head was to the AC-powered TX, the larger C_{b1} was and the smaller C_{b3} was. The relationship where C_{b1} bore an inverse relation to C_{b3} made the return path constant.

We compared results in experiments and simulations with a high frequency structure simulator. The simulation results are also plotted in Figs. 7 and 9. These revealed similar dependencies of path loss on the distance between the TX and the RX on the phantom. The path loss in the experiments was larger than that in the simulations in both results. In fact, the capacitances as shown in Figs. 2 (a) and (b), C_{a4}, C_{b4}, C_{a5} and C_{b5}, were composed of the air gap and plastic sheets that packed the gel material. They attenuated the forward path signal. In contrast, we merely considered that there was a 1 mm air gap between the phantom and the electrode in the simulations. This is estimated to cause the difference in the path loss between the simulations and experiments.

We can obtain approximations ($Loss_{AP1}$ and $Loss_{AP2}$ correspond to the measurement systems for the phantom reclining and standing) from these graphs fitted by the method of least squares as follows:

$$\mathrm{Loss}_{\mathrm{AP1}} = 20 \times \log\left\{0.07 \times \frac{1}{d_1^{1.31}}\right\} [\mathrm{dB}] \qquad (2)$$

$$\mathrm{Loss}_{\mathrm{AP2}} = 20 \times \log\left\{0.15 \times \frac{1}{d_2^{1.48}}\right\} [\mathrm{dB}]. \qquad (3)$$

We considered that the capacitance components of C_{a1} and C_{b1} changed as the distance between the TRXs varied and they mainly caused the changes in path loss. We found it was important to set the minimum received sensitivity and the dynamic range of the received circuit that corresponded to path loss, which had a distance dependence on human body, to enable stable communication between wearable TRXs.

5. CONCLUTION

We proposed communication using NFCC for MHz-band between wearable TRXs on the human body in this paper. Our purpose was to precisely measure signal propagation loss on the human body. Therefore, we developed an EO-OE probe and a battery-powered TX that were the same size as wearable TRXs. We compared methods of measurement using a battery-powered TX and an AC-powered TX. The measured voltages were definitely different for both methods. Consequently, we found that the battery-powered TX and the EO-OE probe could solve the technical problem with overestimating the received signal and we were able to assess the distance dependence of signal loss between transceivers on the human body.

6. ACKNOWLEDGMENTS

Part of this work was supported by a Grant-in-Aid for Scientific Research (A) 23246073 from the Ministry of Education, Culture, Sports, Science and Technology of Japan.

7. REFERENCES

[1] N. Cho, J. Yoo, S. J. Song, J. Lee, S. Jeon, and H. J. Yoo,"The Human Body Characteristics as a Signal Transmission Medium for Intrabody Communication," *IEEE Trans. Microwave Theory and Techniques,* Vol. 55, pp. 1080-1086, May 2007.

[2] A. Fazzi, S. Ouzonov, and J. v. d. Homberg,"A 2.75mW Wideband Correlation-Based Transceiver for Body-Coupled Communication," *IEEE ISSCC,* pp. 204-205, Feb 2009.

[3] J. Bae, H. Cho, K. Song, H. Lee, and H. J. Yoo, "The Signal Transmission Mechanism on the Surface of Human Body for Body Channel Communication," *IEEE Trans. Microwave Theory and Techniques,* Vol. 60, pp. 582-593, March 2012.

[4] T. G. Zimmerman, "Personal Area Networks: Near-field intrabody communication," *IBM Syst. J. ,* Vol. 35, no. 3--4, pp. 609--617, 1996.

[5] Y. Kado, T. Kobase, T. Yanagawa, T. Kusunoki, M. Takahashi, R. Nagai, O. Hiromitsu, A. Hataya, H. Shimasaki, and M. Shinagawa : "Human-Area Networking Technology Based on Near-Field Coupling Transceiver" *2012 IEEE Radio & Wireless Sym. (RWS 2012),* pp. 119 - 122, Santa Clara, California, USA, Jan. 2012.

[6] M. Nozawa, T. Nakamura, H. Simasaki, Y. Kado and M. Shinagawa, "Signal Measurement System Using Electrically Isolated Probe for MHz-Band Near-Field Coupling Communication", *IEEE International Instrumentation and Measurement Technology Conference 2013*, *pp. 37 – 40*, Minneapolis, MN, USA, May. 2013.

[7] N. Haga, K. Saito, M. Takahashi, and K. Ito. 2012. Proper derivation of equivalent-circuit expressions of intra-body communication channels using quasi-static field. *IEICE Trans. Commun*. E95-B, 1, 51-59.

[8] S.Gabriel, R.W.Lau and C.Gabriel, "The dielectric properties of biological tissues: Ⅱ.Measurements in the frequency rage 10 Hz to 20GHz", Phys. Med. Biol. Vol.41, pp. 2251-2269, 1996